A Far-Near Field Transformation Using the Fast Multipole Techniques

Nathalie Bartoli, Francis Collino, Fabrice Dodu, and Thierry Koleck

***Abstract*—We are interested in deducing the coupling between an antenna and some surrounding structures via the only knowledge of the antenna far-field measured in an anechoic room. A new approach based on a multipole expansion of the Green's kernel is considered to evaluate the field in the vicinity of the antenna. Some numerical experiments illustrate the efficiency of the multipole techniques compared to the physical optic approach.**

***Index Terms*—Electric field integral equation (EFIE), fast multipole method (FMM), integral equation, multilevel fast multipole techniques, multipole expansion, near-field to far-field transformation.**

I. Introduction

THE problem under consideration is to determine the coupling of an antenna with surrounding structures of large size from the only knowledge of the antenna far-field measurements. The radiating properties of an antenna are often documented only by measurements in the far zone performed inside an anechoic chamber. The antenna designers are often interested in deducing the coupling of the measured antenna with the surrounding elements in the near zone [1], [2]. Two hypotheses are assumed to obtain the influence of a measured antenna on a surrounding satellite. First, only the influence of the antenna on the satellite structure is taken into account. Next, the satellite is illuminated by the far-field of the antenna measured in some given directions. Hence, the final system is uncoupled and a single equation has to be solved for the current defined on the satellite surface. The associated right-hand side results from the influence of the antenna. To approximate this RHS potential, a classical approach consists in using the far-field in a single direction. It is valid only if the satellite is set in the far zone of the antenna. In contrast, the new method is intended to determine the potential in the vicinity of the antenna from the knowledge of the far-field radiation pattern in all directions. The approach is based on a multipole expansion of the Green's kernel. An interpolation process of the far-field is also introduced. Some numerical experiments are given to illustrate the efficiency and accuracy of the new approach. They also validate our main assumption: the current on the antenna is not too much perturbed by the presence of the satellite.

Manuscript received August 4, 2003; revised February 24, 2004.

N. Bartoli and F. Collino are with European Center for Research and Advanced Training in Scientific Computation (CERFACS), 31057 Toulouse, France (e-mail: bartoli@cerfacs.fr).

F. Dodu was with European Center for Research and Advanced Training in Scientific Computation (CERFACS), 31077 Toulouse, France. He is now with the Physique Corpusculaire et Cosmologie Laboratory, Collège de France, 75231 Paris Cedex 05, France (e-mail: dodu@cdp.in2p3.fr).

T. Koleck is with the Centre National d'Etudes spatiales (CNES), 31401 Toulouse, France (e-mail: Thierry.Koleck@cnes.fr).

Digital Object Identifier 10.1109/TAP.2004.836413

A. Position of the Problem

The problem deals with the coupling of an antenna and a satellite. They are assumed to be both perfectly conducting in order to present the method. But the approach can be applied generally to more complex antennas without difficulty. Using an electric field integral equation (EFIE) formulation, a system of two equations can be set on two surfaces Γ_a and Γ_s describing the antenna and the satellite, respectively

$$\begin{cases} (T_a J_a)(x_a) + (T_s J_s)(x_a) = E^{\text{feed}}(x_a), & x_a \in \Gamma_a \\ (T_s J_s)(x_s) + (T_a J_a)(x_s) = 0, & x_s \in \Gamma_s \end{cases} \quad (1)$$

where E^{feed} is a source term relative to the feeding of the antenna. The two unknowns J_a and J_s are the equivalent currents respectively on Γ_a and Γ_s. In the following, all quantities relative to the antenna (resp. satellite) will be denoted by the index$_a$ (resp. index $_s$). The potential operator T applied to a current J is defined on a boundary Γ by the EFIE operator [3]

$$TJ(x) = iZ_0 k \int_\Gamma G(x,y) J(y) d\Gamma(y) + \frac{iZ_0}{k} \int_\Gamma \text{grad}_x G(x,y) \text{div} J(y) d\Gamma(y) \quad (2)$$

where k is the wave number, Z_0 the vacuum impedance and $G(x,y)$ is the Green's kernel

$$G(x,y) = \frac{\exp(ik|x-y|)}{(4\pi|x-y|)}. \quad (3)$$

The term $\text{div}J$ is the surface divergence of the current J.

B. The Uncoupled System

Generally, the current J_a on the antenna is not significantly affected by the satellite. Therefore, system (1) can be stated in the following weak coupled form

$$\begin{cases} (T_a J_a)(x_a) = E^{\text{feed}}(x_a), & x_a \in \Gamma_a \\ (T_s J_s)(x_s) + (T_a J_a)(x_s) = 0, & x_s \in \Gamma_s \end{cases} \quad (4)$$

where the first equation is related to an isolated antenna. If we assume that this equation can be solved for J_a then J_s can next be obtained simply by solving an equation on Γ_s

$$(T_s J_s)(x_s) = -(T_a J_a)(x_s) \stackrel{\text{def}}{=} -E_a(x_s). \quad (5)$$

In the present study, we furthermore assume that the antenna is only known through its far-field pattern measured in an anechoic

chamber. This quantity is theoretically related to the current J_a flowing at the surface of the antenna Γ_a through

$$E_a^{\infty}(\hat{s}) = \frac{ikZ_0}{4\pi}\left(\int_{\Gamma_a}(\hat{s}\times(J_a(y)\times\hat{s}))e^{-ik\hat{s}\cdot y}d\Gamma_a(y)\right) \quad (6)$$

where $\hat{s}$ is the direction of the measure. We propose two techniques to evaluate $E_a(x_s)$ using directly the antenna far-field measurements. Two other characteristics of the antenna are assumed to be known: its size and c_a the origin relative to its far-field pattern.

C. The Classical and the New Approaches

The first approach issued from the physical optic is based on a far-field approximation of the Green's kernel. When the satellite is far away from the antenna, we can use the far-field approximation to evaluate the field at point x_s on the satellite

$$E_a(x_s) \simeq E_a^{\infty}\left(\frac{(x_s-c_a)}{|x_s-c_a|}\right)\frac{\exp(ik|x_s-c_a|)}{|x_s-c_a|}. \quad (7)$$

This approximation is easy to compute and widely used within the electromagnetism community but it is still valid only if the distance antenna-satellite is large enough. Indeed, this expression of the near-field makes no allowance for the radial component of $E_a(x_s)$. This remark is an important limitation of the approach and will be illustrated by numerical experiments.

The second approach is much more involved. It is based on a multipole expansion of $G(x,y)$, assuming that the satellite and the antenna are more than a quarter of wavelength away from each other: this minimum distance is imposed by the FMM theory [4], [5] and is essential for our application. The algorithm, presented afterward, is adapted from the multilevel fast multipole method (FMM).

These considered approaches raise a few questions. The first one concerns the knowledge of the far-field required in arbitrary directions. As the far-field measurements are given for a fixed number of directions by the data samples, we must introduce some interpolation process. Secondly, to evaluate the near-field at each point of the satellite surface, the new method based on FMM requires more directions of the antenna far-field on the unit sphere that the approach derived from physical optic. We will justify this requirement in terms of accuracy as a function of the distance between the antenna and the satellite. Finally, the assumption leading to the uncoupled problem will be justified by some numerical experiments. All of these points are discussed in the following. Section II presents the interpolation process of the far-field measurements. Section III describes the new approach based on the multipole to compute the near-field on the satellite surface. Some numerical examples are then given in Section IV to validate the new approach compared to the physical optic approximation.

II. The Interpolation Process

The far-field given by measurements is defined on the unit sphere at a fixed number of directions (θ_i,ϕ_j). The two approximations presented below will require the knowledge of the far-field in arbitrary directions. The interpolation process described here is a crucial step for the reconstruction of the near-field, whatever the choice of the approximation. It is based on a spherical mode decomposition, which is a standard technique employed to obtain the antenna far-field pattern from a near-field measurement [1], [2].

A. Determination of the Interpolation Coefficients

The antenna far-field is developed using the spherical harmonic expansion

$$E_{\infty,j}(\hat{s}) = \sum_{l=0}^{\infty}\sum_{m=-l}^{l}\alpha_{l,m,j}Y_{l,m}(\hat{s}) \quad (8)$$

for $\hat{s}$ a direction on the unit sphere and for each component $j=x,y,z$. The spherical harmonics $Y_{l,m}$ constitute a natural basis of the L^2 functions defined on the unit sphere. The series is truncated with $0\le l\le l_{\max}$ and $0\le|m|\le\min(l,m_{\max})$ where the two parameters $l_{\max}$ and $m_{\max}$ are depending on both the frequency and the size of the antenna. If d is the radius of the minimum sphere that encloses the antenna, $l_{\max}$ slightly greater than $|kd|$ appears to be a good parameter for truncation; this can be infered using both the Jacobi–Anger expansion in (6), i.e.

$$\begin{cases} E_a^{\infty}(\hat{s}) = ikZ_0\sum_{l=0}^{\infty}\sum_{m=-l}^{l} i^l(\hat{s}\times\xi_{l,m}\times\hat{s})\,Y_{l,m}(\hat{s}) \\ \xi_{l,m} = \int_{\Gamma_a} j_l(k|y|)J_a(y)\overline{Y_{l,m}\left(\frac{y}{|y|}\right)}d\Gamma_a(y) \end{cases} \quad (9)$$

and the behavior of the spherical Bessel function $j_l(t)$ for l larger than t ($j_l(t)$ decreases to zero exponentially). Let us remark that for compact antennas, the number of terms is very small. In practice, if the far-field is measured with $N_\theta\times N_\phi$ samples, the choice

$$l_{\max} = N_\theta - 1 \text{ and } m_{\max} = \min\left(\left[\frac{(N_\phi-1)}{2}\right], l_{\max}\right) \quad (10)$$

gives us the maximum amount of information about the far-field behavior. The interpolation coefficients $\alpha_{l,m,j}$ are computed with an exact quadrature rule

$$\alpha_{l,m} = \frac{\pi}{N_\theta}\sum_{i=1}^{i=N_\theta} w_i P_l^{|m|}(\cos i_\theta) \times \sin i_\theta \frac{2\pi}{N_\phi}\sum_{j=1}^{j=N_\phi} E_\infty(i_\theta,j_\phi)e^{-imj_\phi} \quad (11)$$

where w_i are the Legendre weights. The determination of w_i is done to integrate the spherical harmonics in the best way. It leads us to choose a rule to integrate the modified Legendre function $P_l^{|m|}(\cos\theta)$ using the far-field measurements [6]. Assuming that the samples ϕ_j are equidistributed, the weights w_i must satisfy

$$\sum_i w_i P_l(\cos\theta_i) = \begin{cases} 2, & \text{if } l=0 \\ 0, & \text{otherwise.} \end{cases} \quad (12)$$

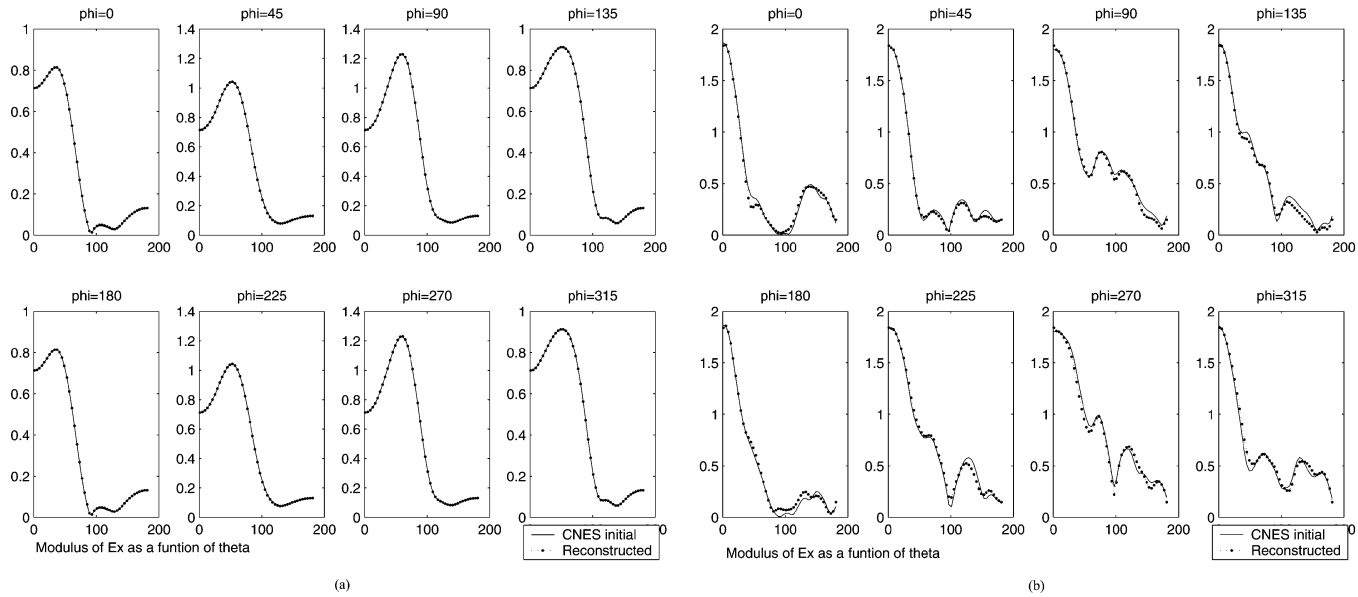

Fig. 1. Modulus of the reconstructed E_x component. (a) Scenario 1: simulation data and (b) scenario 2: measured data.

Thus, the weights are solution of the final system

$$\begin{bmatrix} P_0(\cos\theta_1) & \dots & P_0(\cos\theta_i) \\ P_1(\cos\theta_1) & \dots & P_1(\cos\theta_i) \\ \vdots & \dots & \vdots \\ P_l(\cos\theta_1) & \dots & P_l(\cos\theta_i) \end{bmatrix} \begin{bmatrix} w_1 \\ w_2 \\ \vdots \\ w_i \end{bmatrix} = \begin{bmatrix} 2 \\ 0 \\ \vdots \\ 0 \end{bmatrix} \tag{13}$$

which is solved with a LU or a QR factorization according that the number of measurements is equal or greater than the number or spherical harmonics. Then, the far-field is reconstructed at each point of the unit sphere. The interpolation process is illustrated on two experiments given by two distinctive scenarios. In Fig. 1(a), the data are issued from simulation and in Fig. 1(b), they are given by measurements. In both cases, the reconstructed field is in perfect agreement with the initial one, for all values of (θ, ϕ).

B. The Threshold Procedure

For numerical experiments, we are interested in reducing the number of spherical harmonics. Using the decaying property of $\alpha_{l,m}$ for large (l, m) [7], we introduce a threshold parameter β to eliminate $\alpha_{l,m}$ close to 0 with the following rule shown in (14) at the bottom of the page. To illustrate the process and the choice of β, we consider a far-field given by a plane wave on a dielectric sphere. The angular steps are respectively 1° in θ direction and 10° in ϕ. The relative error on the field components are given in Table I for different values of β.

The number of terms in the series (180×17) is widely reduced by choosing $\beta = 10^{-4}$: only 7×6 terms are required and the error is still relatively small on the three components of the field.

TABLE I
RELATIVE ERROR (L^2 NORM) ON THE FAR-FIELD INTERPOLATION AS A FUNCTION OF β

	without	threshold parameter		
		$\beta = 10^{-2}$	$\beta = 10^{-3}$	$\beta = 10^{-4}$
$l_{\max}$ - $m_{\max}$	180 - 17	4 - 5	5 - 5	7 - 6
error E_x	0.011%	1.65%	0.22%	0.026%
error E_y	0.019%	0.87%	0.14%	0.015%
error E_z	0.007%	2.10%	0.20%	0.032%

III. THE MULTIPOLE APPROXIMATION

We describe the new approach to evaluate the electric field produced by the antenna at the surface of the satellite using the antenna far-field measurements.

A. The Expression of the Near-Field

The main idea is derived from the multilevel FMM. The fast multipole algorithms are known to provide an efficient way to compute the electromagnetic field from the knowledge of the current. If J_a were known, the computation of $E_a(x_s)$

$$E_a(x_s) = iZ_0k \int_{\Gamma_a} G(x_s, y) J_a(y) d\Gamma_a(y) + \frac{iZ_0}{k} \int_{\Gamma_a} \mathrm{grad}_{x_s} G(x_s, y) \mathrm{div} J_a(y) d\Gamma_a(y) \tag{15}$$

may be done for each point x_s on Γ_s, with $s = 1, \dots, N_s$, with N_s the number of considered points. Instead of performing all of those N_s calculations, we use a specific distribution of the points in an octree structure and an approximation of the kernel. We

$$\alpha_{l,m,j} = \begin{cases} \alpha_{l,m,j}, & \text{if } \alpha_{l,m,j} \geq \beta \max_{l,m}(\alpha_{l,m,j}) \text{ for } 0 \leq l \leq l_{\max} \text{ and } -l \leq m \leq l \\ 0, & \text{otherwise.} \end{cases} \tag{14}$$

construct a cubic octree around the satellite. We start with a large cube enclosing the satellite; this cube is partitioned into eight smallest cubes and then each subcube is recursively subdivided into smaller cubes until the edge length of the smallest cube is about a quarter of wavelength. We note by $c_{B_{x_s}}$ the center of the cube containing the point x_s. By using the addition theorem of Gegenbauer for the Green's kernel [4], [6] and usual techniques of FMM, we rewrite the near-field expression in the following form:

$$E_a(x_s) \simeq \frac{k}{4\pi} \int_{\mathcal{S}} E_a^{\infty}(\hat{s}) T^L(\hat{s}, D) e^{+ik(x_s - c_{B_{x_s}})\cdot\hat{s}} d\sigma(\hat{s}) \quad (16)$$

where $\mathcal{S}$ is the unit sphere. If $D = c_{B_{x_s}} - c_a$, the involved term $T^L(\hat{s}, D)$ is the operator to transfer information from $c_{B_{x_s}}$ to c_a

$$T^L(\hat{s}, D) = -i \sum_{\ell=0}^{L} i^{\ell}(2\ell+1) h_{\ell}^{(1)}(k|D|) P_{\ell}(\hat{D}\cdot\hat{s}) \quad (17)$$

$P_\ell(x)$ is the Legendre polynomial of order ℓ, $h_\ell^{(1)}(u)$ is the spherical Hankel function of order ℓ and the parameter L determines the number of terms in the Gegenbauer series. The quality and the accuracy of the approximation depend on the choice of L. We have several formulae at our disposal in the literature [8], [9] to force the truncation error to be arbitrarily small. In our study, we use

$$L = L(\epsilon, kd) = kd + C_\epsilon \log(kd + \pi) \quad (18)$$

where d is the size of the largest cube and C_ϵ is a constant equal to 5 for a given precision of $\epsilon = 10^{-6}$ ($kd < 60$). However, a minimum distance between x_s and the antenna is required to overcome over flows in finite arithmetic [10], [11]: we assume that a quarter of wavelength separates the two obstacles.

Formula (16) has a profound meaning. The near-field can be retrieved at each point x_s well separated from the antenna, via the only knowledge of the far-field pattern. The error of this approximation is directly linked to the choice of L. Compared to the exponential approach (7), we perform here an integral over the unit sphere, so all directions (θ, ϕ) are taken into account to evaluate $E_a(x_s)$. This is a main difference with the usual approximation. From a practical point of view, all techniques developed in the context of FMM are used: construction of an octree, translation procedure and disaggregation of radiating fields… [4]–[6], [12]. Let us remark that the system antenna + satellite is considered, so the number of multipoles is fixed with

$$L_{\text{sys}} = L + l_{\max}. \quad (19)$$

On the one hand, the antenna far-field is considered as the sum of $l_{\max}$ spherical harmonics. On the other hand, the function $\exp(+ik(x_s - c_{B_{x_s}}))$ with $|x_s - c_{B_{x_s}}| < d$ is approximately equal to a sum of $L(\epsilon, kd)$ spherical harmonics [see Definition (18)]. Hence, the product of the two functions in (16) is almost a sum of harmonic functions of degree less than $L(\epsilon, kd) + l_{\max}$. This is why we choose the number of multipoles L in (16) equals to L_{sys}.

As the CPU time of the FMM algorithm is widely dependent on the number of multipoles, the threshold procedure introduced in Section II-B is particularly interesting to decrease $l_{\max}$ and therefore L_{sys}.

IV. Numerical Experiments

For the numerical aspects, we use some classic tools of integral equations. The satellite surface is meshed with triangles and we use the MOM method [3], [13] to get the linear system

$$Z_s I_s = U_a \quad (20)$$

where Z_s is the impedance matrix relative to the satellite and I_s defines the flux of the current density through the edges of the triangles. The potential U_a is directly linked to the applied field E_a

$$(U_a)_j = -\int_{\Gamma_s} E_a(x)\varphi_j(x) d\Gamma_s(x) \quad (21)$$

where φ_j is the RWG test basis function associated to edge j [14]. Finally, the linear system (20) is solved by using a direct (LU decomposition) or an iterative (coupling FMM-GMRES) solution. From the knowledge of I_s, the radiation pattern can be plotted.

We consider some examples to validate and compare the two approximations. For the interpolation process, the threshold parameter β is carried out to get a relative error lower than 0.2% between each component of the initial far-field and the reconstructed one. This choice is justified in the following.

In a first example, the antenna is a simple dipole located at some distance on the x axis. In this case, U_a can be computed analytically. The wave number equals 12, the number of degrees of freedom is 25 232 (with 10 points per wavelength) and the geometry is shown in Fig. 2. Table II reports the relative quadratic errors obtained for approximations (7) (EXP approach) and (16) (FMM approach) for two different values of the distance between the antenna and the satellite.

The efficiency of the FMM approximation is observed even for small distance. As previously mentioned, the EXP approach is valid only for a distance larger than 2λ to ensure an error lower than 10%. To evaluate the error induced on the current, we solve (20). For the FMM approximation at distance 0.3λ, the error is equal to 0.998% for I_s and 0.006% for the radiation pattern. The accuracy obtained on these quantities validates the FMM approach. The good agreement obtained for the radiation pattern is illustrated in Fig. 3.

In a second example, the antenna is a dielectric sphere of permittivity $\varepsilon = 2$ illuminated by a plane wave, and the satellite is a perfectly conducting sphere at 2λ away from the antenna. For this example, we have generalized the approach to dielectric antennas. The exact near field is now computed from the knowledge of the electric and magnetic currents J_a and M_a

$$\begin{aligned} E_a(x_s) = {} & iZ_0 k \int_{\Gamma_a} G(x_s, y) J_a(y) d\Gamma_a(y) \\ & + \frac{iZ_0}{k} \int_{\Gamma_a} \text{grad}_{x_s} G(x_s, y) \text{div} J_a(y) d\Gamma_a(y) \\ & + \int_{\Gamma_a} \text{grad}_y G(x_s, y) \times M_a(y) d\Gamma_a(y). \end{aligned} \quad (22)$$

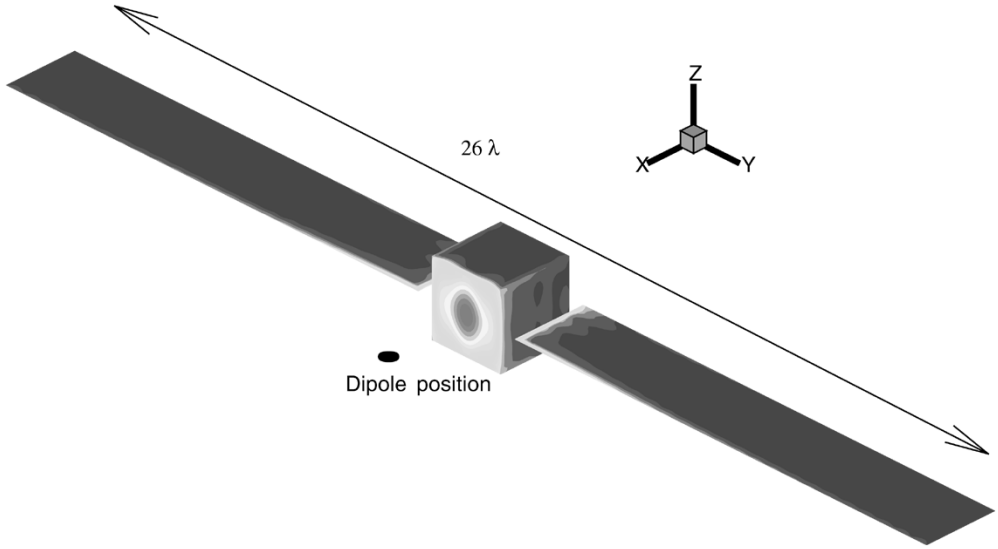

Fig. 2. Current on the satellite surface excited by a dipole.

TABLE II
RELATIVE QUADRATIC ERROR ON U_a AS A FUNCTION OF THE DISTANCE ANTENNA-SATELLITE

Reference Potential = analytic dipole		
distance antenna–satellite	0.3λ	7λ
EXP approach	33.74 %	2.54 %
FMM approach	0.26 %	0.002 %

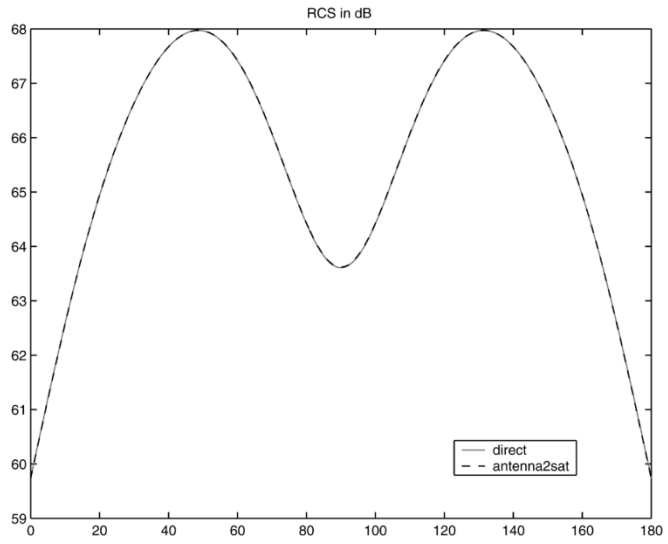

Fig. 3. Radiation pattern of the satellite when the distance dipole-satellite equals 0.3λ.

The errors on U_a between the exact solution (22) and the approximations (7) and (16) are respectively given by 9.33% (EXP) and 0.017% (FMM).

The third example concerns a more realistic case. The antenna is defined by four helicoidal wires and each wire is fed in phase quadrature by a delta-gap as illustrated in Fig. 4(a). The dimensions of this antenna are 0.2λ in height and 0.14λ in diameter. In a first step, the wave number equals 1.5 in order to consider few mesh points and the satellite is simply represented by a perfectly conducting unit sphere. The purpose is to study the interpolation of the antenna far-field, the threshold procedure and its influence on the FMM approach to evaluate U_a. A first data samples for the far-field measurements is considered: the angular step $\Delta\theta$ is fixed at 1° for $\theta \in [0,180]$ and $\Delta\varphi$ equals 4.5° with $\varphi \in [0,360]$. In Table III, we give the error on the interpolation process as a function of β. By keeping the two highest values of β, we report in Tables IV and V, the error on U_a between the FMM approach and the direct computation for different distances between the antenna and the sphere: λ, 2λ, and 23λ.

The choice of β is important for the determination of the near-field on the satellite surface when the FMM approach is used. The error on U_a increases considerably when β equals 10^{-3}. We generally fix β so as to get a relative error on the interpolated far-field lower than 0.2% on the three components. In the present case, this rule leads us to take $\beta = 5.5 \times 10^{-4}$ and ensures an error on U_a lower than 1%. We proceed with the influence of the data samples. We keep the same configuration (helicoidal antenna and metallic sphere) and consider now a coarser grid for the data samples ($\Delta\theta = 1^\circ, \Delta\varphi = 36^\circ$). For comparison with the previous case, the error on U_a is given in Table VI. With a coarse angular step on φ, the error increases but is still less than 5% on the right-hand side, which could be sufficient in some applications. If more accuracy is required, the far-field of the helicoidal antenna must be described with enough measured data. In our experiments, we remark that $\Delta\theta$ must be about 1° or 2° and $\Delta\varphi$ lower than 10°.

In a second step, we keep the helicoidal antenna measured on a fine grid with $\Delta\theta = 1^\circ$ and $\Delta\varphi = 4.5^\circ$ and we increase the frequency with $k = 13$. The satellite is now constituted by different perfectly conducting elements: a square box, some solar panels and cylindrical objects as shown in Fig. 4(b). The dimensions are about $8\lambda \times 16\lambda \times 12\lambda$. The number of degrees of freedom is 7859 by using 10 points by wavelength. Three positions of the satellite are considered: the satellite is located at, respectively, $\lambda/4$, λ, and 10λ from the antenna. Table VII reports the relative quadratic error obtained with the two different approximations. All results obtained by the FMM approach are

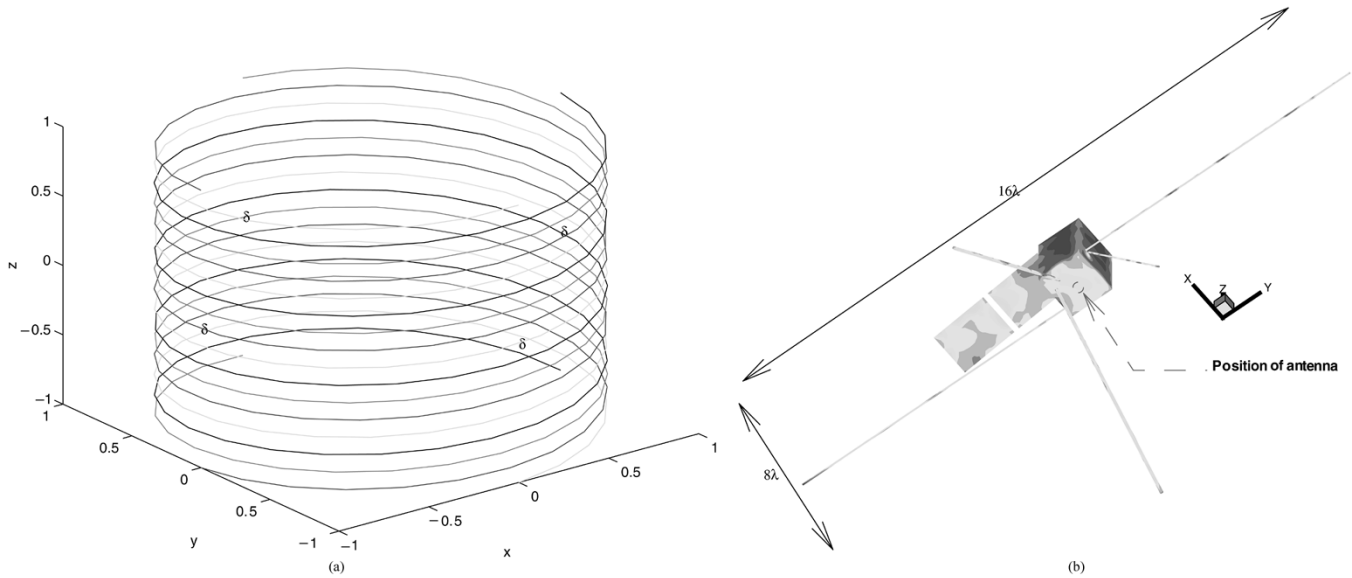

Fig. 4. Configuration antenna–satellite. (a) Quadrifilar helicoidal antenna and (b) satellite.

TABLE III
RELATIVE QUADRATIC ERROR BETWEEN THE INITIAL FAR-FIELD OF THE HELICOIDAL ANTENNA AND ITS INTERPOLATED FIELD AS A FUNCTION OF β

	$\beta = 10^{-3}$	$\beta = 5.5 \times 10^{-4}$	$\beta = 10^{-4}$	without
$l_{\max}$ - $m_{\max}$	7 - 2	7 - 4	8 - 6	180 - 39
error $(E_\infty)_x$	1.089%	0.053%	0.008%	0.002%
error $(E_\infty)_y$	1.077%	0.066%	0.009%	0.003%
error $(E_\infty)_z$	2.410%	0.110%	0.016%	0.003%

TABLE IV
RELATIVE QUADRATIC ERROR ON U_a AS A FUNCTION OF THE DISTANCE ANTENNA-SATELLITE WHEN $\beta = 5.5 \times 10^{-4}$

Reference Potential = direct computation (15)			
distance antenna–satellite	λ	2λ	23λ
EXP approach	67.69%	28.67%	3.17%
FMM approach	0.95%	0.93%	0.89%

TABLE V
RELATIVE QUADRATIC ERROR ON U_a AS A FUNCTION OF THE DISTANCE ANTENNA-SATELLITE WHEN $\beta = 10^{-3}$

Reference Potential = direct computation (15)			
distance antenna–satellite	λ	2λ	23λ
EXP approach	68.71%	28.01%	3.68%
FMM approach	3.51%	3.05%	2.60%

TABLE VI
RELATIVE QUADRATIC ERROR ON U_a AS A FUNCTION OF THE DISTANCE ANTENNA-SATELLITE WITH A COARSE GRID WHEN $\beta = 5.5 \times 10^{-4}$

Reference Potential = direct computation (15)			
distance antenna–satellite	λ	2λ	23λ
EXP approach	68.65%	27.97%	3.64%
FMM approach	3.94%	3.12%	2.63%

TABLE VII
RELATIVE QUADRATIC ERROR ON U_a AS A FUNCTION OF THE DISTANCE ANTENNA-SATELLITE WHEN $k = 13$

Reference Potential = direct computation (15)			
distance antenna–satellite	$\lambda/4$	λ	10λ
EXP approach	47%	21.12%	2.31%
FMM approach	0.34%	0.10%	0.02%

TABLE VIII
RELATIVE QUADRATIC ERROR ON I_s AS A FUNCTION OF THE DISTANCE ANTENNA-SATELLITE WHEN $k = 13$

distance antenna–satellite	$\lambda/4$	λ	10λ
FMM approach	0.63%	0.73%	0.28%
coupled or uncoupled system	0.02%	0.01.%	0.0001%

very efficient, particularly when the distance antenna-satellite is $\lambda/4$. As previously, we give the relative errors on current I_s for the FMM approach in Table VIII.

In order to justify our main assumption leading to the uncoupled problem, we report also the relative error between the solution of the coupled problem (1) and the solution of the uncoupled one using a direct solver for (20) where the right-hand side is given by (15). The errors given in Table VIII justify our assumption: the uncoupled error is negligible compared to the error induced by the FMM approximation. Thus, the current on the antenna is not too much perturbed by the presence of the satellite even if the two obstacles are a quarter of wavelength away.

For the last numerical experiment, we keep the previous geometrical configuration and we increase the frequency. Now the wave number equals 27 and 46 793 degrees of freedom are used for the satellite. The dimensions are now $17.5\lambda \times 3.5\lambda \times 13\lambda$ for the satellite and $0.43\lambda \times 0.3\lambda$ for the antenna. The far-field is measured with $\Delta\theta = 1^\circ$ and $\Delta\varphi = 4.5^\circ$. Table IX reports the relative quadratic error obtained for U_a between approximations (7) and (16). We obtain very good results. For instance when the distance is $\lambda/4$, we plot in Fig. 5 the radiation pattern obtained from the fine grid compared with the radiation pattern induced by a coarser grid to measure the antenna far-field.

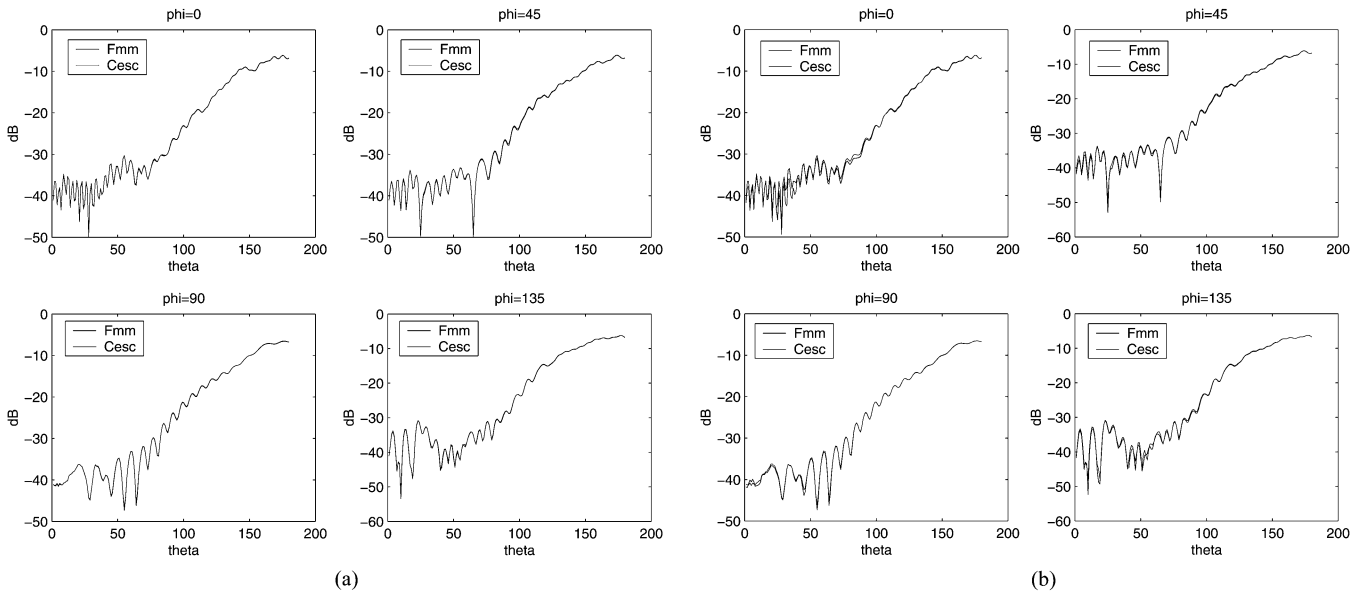

Fig. 5. Radiation pattern (dB) of the satellite when the distance antenna-satellite equals $\lambda/4$ as a function of the angular step on the measured far-field. (a) Fine grid $\Delta\theta = 1^\circ \quad \Delta\varphi = 4.5^\circ$. (b) Coarse grid $\Delta\theta = 1^\circ \quad \Delta\varphi = 45^\circ$.

TABLE IX
RELATIVE QUADRATIC ERROR ON U_a AS A FUNCTION OF THE DISTANCE ANTENNA-SATELLITE WHEN $k = 27$

Reference Potential = direct computation (15)			
distance antenna–satellite	$\lambda/4$	λ	10λ
EXP approach	56.60%	54.13%	35.31%
FMM approach	3.28%	2.08%	2.005%

TABLE X
TIME AND MEMORY SIZE FOR THE DIRECT CODE TO CALCULATE I_s

	7859 degrees of freedom	**46 793** dof
Assembly	5 min 48 s	6 h 8 min
LU solution	1 h 5 min	243 h 10 min
CPU Time global	1 h 10	250 h (SGI Origin)
Size (in Megabytes)	1024	35 840

TABLE XI
TIME AND MEMORY SIZE FOR THE COUPLING OF THE FAR TO NEAR-FIELD TRANSFORMATION WITH THE FMM ALGORITHM TO CALCULATE I_s

	7859 dof	**46 793** dof
Far to near-field	1 min	2 min
Preconditioner	1 min 48 s	1 h 21 min
Matrix-vector product	2 s 30	17 s 64
Number of iterations residual=0.42×10^{-3}	99	300
GMRES solution	4 min 10 s	1 h 44 min
CPU Time global	7 min	3 h
Size (in Megabytes)	30	114

This example illustrates that sufficient accuracy can be obtained on the radiation pattern using a coarse grid when the antenna and the satellite are very close.

In terms of computation requirements, the memory size and time used by the transformation far to near-field coupled with the FMM code is without comparison with the direct code as reported in Tables X and XI. The comparison is carried out on a single processor of a COMPAQ SC40 with 48 GB memory, running at 1 GHz.

V. CONCLUSION

In this paper, we present a new approach involving FMM techniques to compute the near-field on a satellite from the measured far-field of a surrounding antenna. This far to near-field transformation requires the interpolation of the far-field measurements to get them in arbitrary directions. A threshold parameter is introduced to reduce the number of interpolation coefficients and the CPU time of the FMM approach too. The first results are promising, particularly the experiments on the quadrifilar helicoidal antenna. In the future, we plan to develop an hybrid method to consider some practical situations where the antenna is on the satellite surface. In this case, an exact computation of the field could be done for the points of the satellite close to the antenna and a multipole approach will be envisaged for distant contributions.

ACKNOWLEDGMENT

The authors would like to acknowledge the CINES for granting access to its computational facilities.

REFERENCES

[1] J. E. Hansen, *Spherical Near-Field Antenna Measurements*, ser. IEE Electromagnetics waves 26. Stevevage, U.K.: Peregrinus, 1988.
[2] S. Blanch, J. Romeu, and A. Cardama, "Near field in the vicinity of wireless base-sation antennas: An exposure compliance approach," *IEEE Trans. Antennas Propagat.*, vol. 50, pp. 685–692, 2002.
[3] J. Jin, *The Finite Element Method in Electromagnetics*, 2nd ed. New York: Wiley, 2002.
[4] W. Chew, J. Jin, E. Michielssen, and J. Song, Eds., *Fast and Efficient Algorithms in Computational Electromagnetics*. Boston, MA; London, U.K.: Artech Antennas and Propagation Library, 2001.

[5] F. Collino and F. Millot, "La Méthode multipôle pour les problèmes de diffraction," CERFACS, Toulouse, France, Tech. Rep. TR/EMC/00/95, 2000.
[6] E. Darve, "The fast multipole method: Numerical implementation," *J. Comput. Phys.*, vol. 160, no. 1, pp. 196–240, May 2000.
[7] A. G. Ramm, "Stability estimates in inverse scattering," *Acta Appl. Math.*, vol. 28, no. 1, pp. 1–42, 1992.
[8] Q. Carayol, "Développement et analyse d'une méthode multipôle multi-niveaux pour l'électromagnétisme," Ph.D. dissertation, Université Paris, 2002.
[9] R. Coifman, V. Rokhlin, and S. Wandzura, "The fast multipole method for the wave equation: A pedestrian prescription," *IEEE Antennas Propagat. Mag.*, vol. 35, pp. 7–12, June 1993.
[10] M. A. Epton and B. Dembart, "Multipole translation theory for the three-dimensional Laplace and Helmholtz equations," *SIAM J. Sci. Comput.*, vol. 16, no. 4, pp. 865–897, 1995.
[11] J. Song, C. Lu, and W. Chew, "Multilevel fast multipole algorithm for electromagnetic scattering," *IEEE Trans. Antennas Propagat.*, vol. 45, pp. 1488–1493, 1997.
[12] G. Sylvand, "La Méthode multipôle rapide enélectromagnétisme: performances, parallélisation, applications," Ph.D. dissertation, ENPC, Paris, France, 2002.
[13] R. F. Harrington, *Field Computation by Moment Methods*. New York: MacMillan, 1968.
[14] S. M. Rao, D. R. Wilton, and A. W. Glisson, "Electromagnetic scattering by surfaces of arbitrary shape," *IEEE Trans. Antennas Propagat.*, vol. AP-30, pp. 409–418, May 1982.

Nathalie Bartoli was born in France in 1974. She received the Eng. diploma and Ph.D. degree in applied mathematics from the National Institute of Applied Sciences of Toulouse, France, in 1997 and 2000, respectively.

From 2002 to 2003, she joined the CAIMAN project at INRIA Sophia-Antipolis (French National Institute for Research in Computer Science and Control). She is currently a Researcher on the Electromagnetism Team at CERFACS (European Center for Research and Advanced Training in Scientific Computation) in Toulouse. Her research interests include computational electromagnetics, especially numerical techniques involving frequency integral equations. At present, she is working on coupling finite elements and integral equations with an adaptative absorbing boundary condition.

Francis Collino was born in 1958. He received the Eng. Degree from École Nationale Supérieure des Mines, Paris, France, in 1982 and the Ph.D. degree in applied mathematics from the University Paris Dauphine, France, in 1987.

In 1983, he was with IFP French National for Oil Institute. From 1987 to 1997, he was with the Institut National en Informatique et Automatique (INRIA), working on the ONDES project. Since 1997, he has been established as a Consultant working with the European Center for Research and Advanced Training in Scientific Computation (CERFACS) and the Commissariat à l'Energie Atomique (CEA)–d'études Scientifiques et Techniques d'Aquitaine (CESTA). He has authored or coauthored papers in various directions including domain decomposition, absorbing boundary conditions, perfectly matched layers, mesh refinement, fictitious domain methods, integral equations, multipoles, and paraxial equations. His domains of interest include mathematical modeling and numerical analysis of wave propagation phenomena with applications to various areas of physics (acoustic, elasticity, and electromagnetism).

Fabrice Dodu received the Ph.D. degree in applied mathematics from the the National Institute of Applied Sciences of Toulouse, Toulouse, France, in 2000, with a dissertation on the approximation and interpolation of vector fields.

He was an Engineer on the Electromagnetism and Control Team of the European Center for Research and Advanced Training in Scientific Computation (CERFACS), Toulouse, France. Since 2004, he has been a Research Engineer in the Physique Corpusculaire et Cosmologie laboratory, Collège de France, Paris, focusing on high performance computing for astro-physics, particularly in the study of cosmic microwave background and the European Space Agency (ESA).

Thierry Koleck received the M.Sc. degree from the University of Toulouse, France, and the Ph.D. degree from the University of Paris, France, in 1993 and 1998, respectively.

Since 1997, he has been with the Centre National d'Etudes spatiales (CNES), the French space agency in Toulouse as an Antenna Enginner. He has been involved in research and development of space antennas for many satellite projects. His interests include space antennas, numerical methods for antenna analysis, antenna/structure interaction analysis, and optimization methods.